Multiple Numerical Solutions of Laminar Fuel-rich Spray Flame Structures in the Counterflow Configuration

Z. Ying, E. Gutheil*

[1]Interdisciplinary Center for Scientific Computing, Heidelberg University
69120 Heidelberg, Germany
*Corresponding author: gutheil@iwr.uni-heidelberg.de

Abstract
Multiple structures of laminar non-premixed ethanol/air spray flames under fuel-rich conditions in the axisymmetric counterflow configuration are studied numerically. A monodisperse ethanol spray carried by air is directed against an opposed air stream. Both enter at 300 K and the system is at atmospheric pressure. Up to three different spray flame structures may exist for the same boundary and initial conditions depending on the initial droplet size, the strain rate, and the equivalence ratio. Regime diagrams are presented and discussed to display the conditions under which the multiple structures exist. The most stable spray flames consist of two chemical reaction zones where one resides on the spray side and another one on the gas side of the configuration. Moreover, spray flames with single chemical reaction zones are found which may reside either on the spray or on the gas side of the configuration, depending on the boundary conditions. Mechanisms for the breakdown of the different types of spray flame structures are discussed. The present study aims to contribute to an improved understanding of these spray flame structures under fuel-rich conditions.

Keywords
Multiple Solutions, Spray flame structure, Laminar fuel-rich spray flames, Counterflow configuration

Introduction

Spray flames are relevant in many practical combustion systems such as industrial furnaces, aircraft engines, household burners, and internal combustion engines [1]. In turbulent spray flames, the consideration of detailed chemical reactions is inevitable to study pollutant formation. For this purpose, the spray flamelet concept has been introduced [2, 3]. A laminar spray flamelet library is generated which are stretched and folded to account for the turbulence [4]. Laminar flame structures are the basis of several flamelet models developed for the simulation of turbulent gas flames in a computationally cost-effective way [5, 6, 7]. For spray flames, these models have been less investigated, since more parameters are required for characterizing the spray flamelets, making these models particularly complex [2, 3]. Moreover, the possibility of the existence of multiple numerical solutions for a specific set of boundary and initial conditions strongly influences the formulation of spray flamelet models, which requires more research.
Continillo and Sirignano [8] postulated that the governing equations of the laminar counterflow spray flames might have multiple numerical solutions. Gutheil [9] first numerically confirmed the existence of two different solutions for the same initial and boundary conditions for low strain rates for stoichiometric methanol/air spray flames. Vié et al. [10] identified the bifurcation of a monodisperse n-dodecane spray and revealed multi-modal spray flame structures which directly affect flamelet-based tabulation methods. Xie et al. [11] exhibited the coexistence of collocated, distributed, and cool flames when they numerically studied canonical counterflow spray flames at relatively low strain rates using different low-temperature chemical reaction mechanisms. Carpio et al. [12] studied dodecane spray flames with carrier nitrogen against an air stream using a one-step chemical reaction, and they identified two solutions where one is a diffusion flame and the second is flameless.

Most aforementioned studies concern spray flames at a global stoichiometric equivalence ratio even though locally fuel-rich or lean conditions may prevail. Ying et al. [13] recently identified two different spray flame structures in the counterflow configuration under fuel-rich conditions. The present study is an extension of that work, and a third spray flame structure is found, residing on the spray side of the configuration within the spray vaporization zone. The present study identifies conditions under with these different flame structures coexist.

Results and Discussion

Numerical simulations are performed for a monodisperse ethanol spray with carrier gas air directed against an air stream. The governing equations are the same as reported by Continillo and Sirignano [8] and modified by Gutheil and Sirignano [14] to account for detailed chemical reactions and variable transport properties. The system is at atmospheric pressure with initial gas and the spray temperatures of 300 K and a global equivalence ratio of 1.1 through 1.6 on the spray side of the configuration. Structures of fuel-rich spray flames with initial droplet radii ranging from 10 μm to 50 μm and an initial spray velocity $v_{-\infty} = 0.44$ m/s at a spray-sided gas strain rate of 55/s are investigated. Gas strain rates up to the values beyond which no solutions are achieved are studied.

First, regime diagrams are presented to show the conditions under which multiple spray flame structures exist and then these structures are presented and discussed in more detail.

Existence of multiple structures of fuel-rich spray flames

Multiple structures of the spray flames may exist for different initial droplet radii and gas strain rates for fixed equivalence ratio of the monodisperse spray. Diagrams for the existence of the multiple spray flame structures for initial droplet radii, R_0 of 10 μm, 30 μm, and 50 μm, cf. Fig. 1a through 1c are generated for the same initial and boundary conditions where both the equivalence ratio and the gas strain rate on the spray side of the configuration are varied. The blue and red triangles display structures with a single chemical reaction zone that resides on the spray and the gas side of the configuration, respectively, and the circle shows conditions for which structures with two reactions zones exist, where one resides on the spray side and the other one on the gas side of the counterflow configuration. Thus, up to three spray flame structures may coexist for the same boundary conditions.

A comparison of the structures displayed in Fig. 1 shows that the flame structures with two reaction zones are more stable than these with single chemical reaction zones. If multiple structures exist, the single chemical reaction zone on the gas side of the configuration is preferred for larger initial droplet sizes whereas the spray structures with a spray-sided single chemical reaction exists mainly for the spray flames with the smallest initial droplet size of 10 μm. Triple structures coexist only for small initial droplet radii at moderate strain rates.

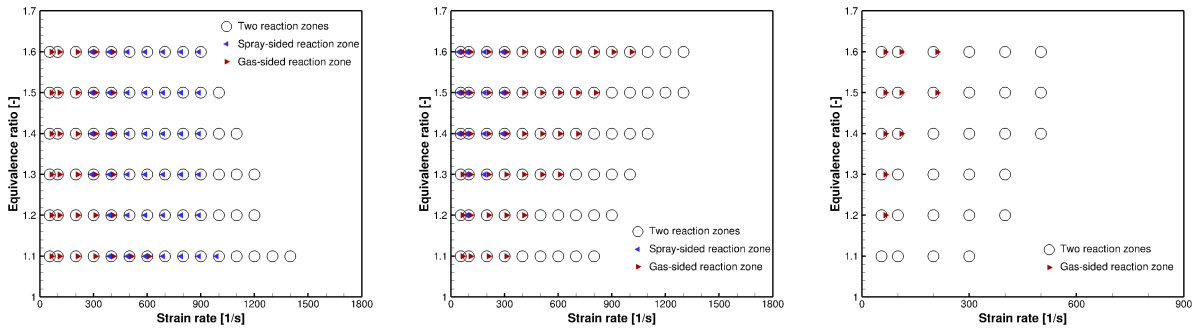

(a) $R_0 = 10\,\mu\text{m}$ (b) $R_0 = 30\,\mu\text{m}$ (c) $R_0 = 50\,\mu\text{m}$

Figure 1. Regime diagrams for multiple flame structures.

Analysis of the spray flame structures

The different flame structures will be presented and discussed for a fixed equivalence ratio of 1.4. Since there is not fixed gas strain rate for which all possible structures for different initial droplet radii exist, the triple structure is presented for $a_{-\infty} = 400/\mathrm{s}$ and $R_0 = 10\,\mu\mathrm{m}$, whereas the other structures are evaluated at 500/s.

Figure 2 shows the triple flame structures for the same initial and boundary conditions of $R_0 = 10\,\mu\mathrm{m}$, $E_\mathrm{r} = 1.4$, $T_{\mathrm{l},0} = T_{\mathrm{g},0}$ = 300 K, $a_{-\infty} = 400/\mathrm{s}$, where the upper parts display the outer flame structures and the lower parts the mass vaporization rate, S_v and the gas and droplet velocities of the monodisperse spray. Figure 2a shows the most stable solution with two chemical reactions zones one of which resides on the spray and the other one on the gas side of the counterflow configuration. The spray completely evaporates near the stagnation plane at $y = 0$, where a dip in the profile of the gas temperature is visible that accounts for the strong energy consumption related to spray evaporation rate, which peaks near that location. The strong influence of drag force on the droplets leads to the difference in gas and droplet velocities shown in the lower part of Fig. 2a.

Two different spray flame structures are found with single chemical reaction zones for the same conditions. In Fig. 2b, the reaction zone resides on the gas side of the configuration whereas in Fig. 2c, it locates on the spray side. The principal spray flame structure with separated vaporization and reactions zones, cf. Fig. 2b, was already identified by Ying et al. [13] for $a_{-\infty} = 55/\mathrm{s}$, $E_r = 1.5$, and $R_0 = 50\ \mu\mathrm{m}$ for which the third structure in Fig. 2c does not exist.

Gutheil [9] identified the two different spray flame structures of methanol/air sprays that show two chemical reaction zones and one on the spray side of the configuration, and it was argued that the spray-sided chemical reaction zones are similar or even identical with the gas-sided reaction zone being extinguished in the situation with a single chemical reaction zone on the spray side. This is confirmed in the present study, cf. Figs. 2a and 2c. The additional structure shown in Fig. 2b was not identified in the earlier study [9], and the comparison of the peak temperatures in Figs. 2a and 2b reveals that the flame with a single chemical reaction zone is considerably colder than that with the two chemical reaction zones, which is due to the large separation distance of the vaporization and reaction zones in Fig. 2b, where the gas flame is

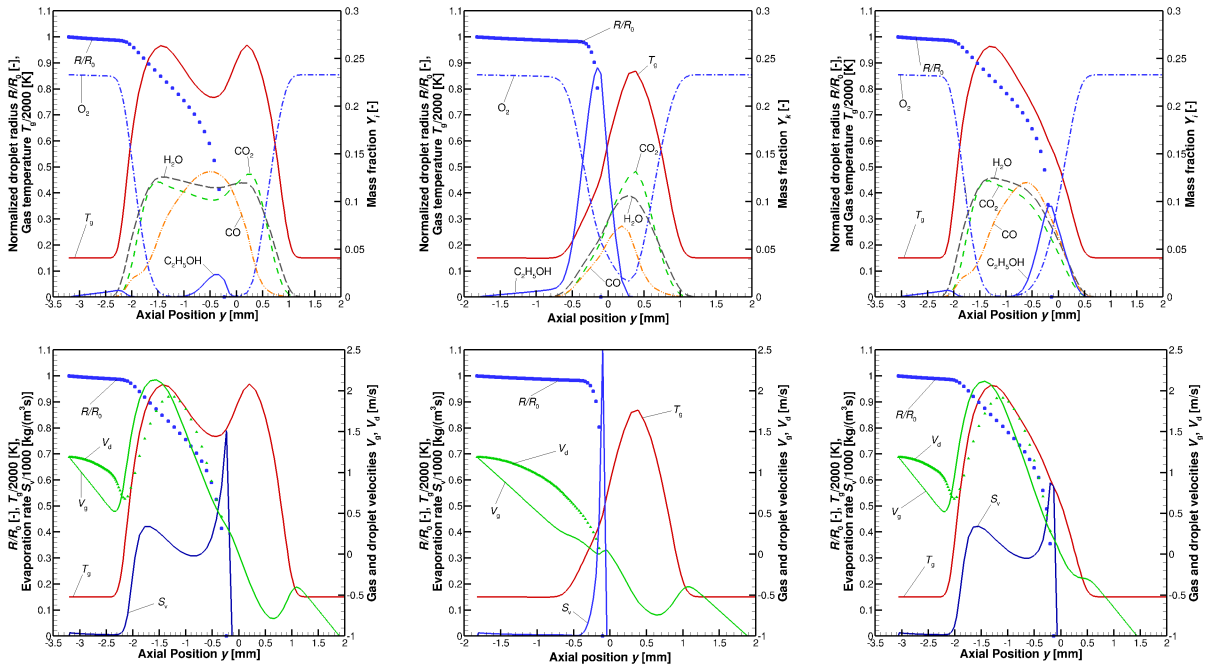

(a) Two reaction zones (b) Single reaction zone on the gas side (c) Single reaction zone on the spray side

Figure 2. Multiple spray flame structures for $R_0 = 10\,\mu\mathrm{m}$, $E_\mathrm{r} = 1.4$, $T_{\mathrm{l},0} = T_{\mathrm{g},0}$ = 300 K, $a_{-\infty} = 400/\mathrm{s}$. Upper part: Outer flame structure; Lower part: Spray characteristics.

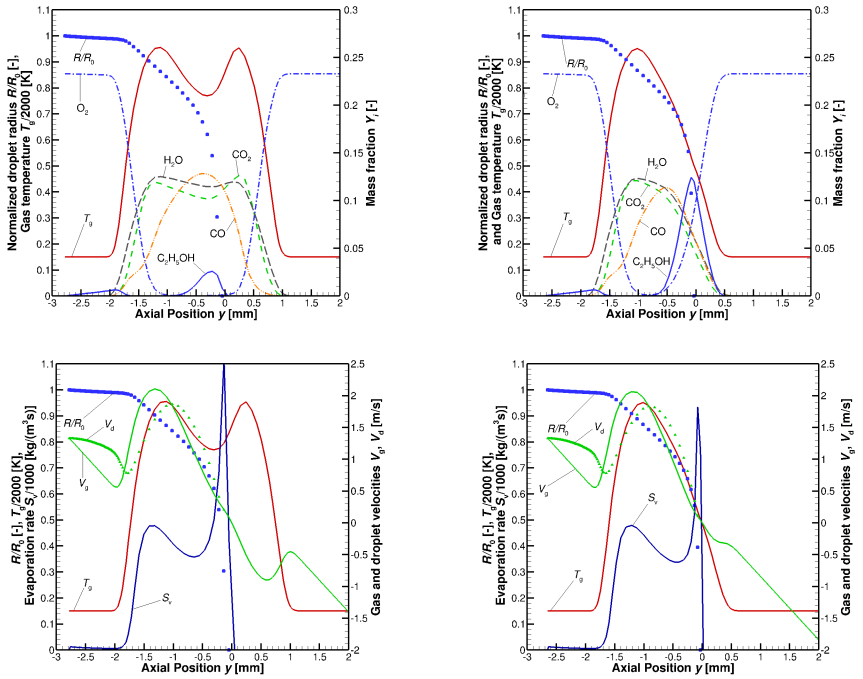

(a) Two reaction zones (b) Single reaction zone on the spray side

Figure 3. Multiple spray flame structures for $R_0 = 10\,\mu\text{m}$, $E_\text{r} = 1.4$, $T_{\text{l},0} = T_{\text{g},0}$ = 300 K, $a_{-\infty}$ = 500/s. Upper part: Outer flame structure; Lower part: Spray characteristics.

not fed with fuel vapor to sustain combustion. As the gas strain rate is increased further, this chemical reaction zone will break down due to the low peak gas temperature of about 1700 K, and the evaporation zone is more and more separated from the main reaction zone, which can be seen from the profile of S_v in the lower part of Fig. 2b. Therefore, only flame structures with two chemical reaction zones and with one reaction zone on the spray side are found for $a_{-\infty}$ = 500/s, see Fig. 1.

Figures 3 through 5 display the different spray flame structures that exist at $E_r = 1.4$, $a_{-\infty} = 500/\text{s}$ for the different initial droplet radii of $R_0 = 10\,\mu\text{m}$, $30\,\mu\text{m}$, and $50\,\mu\text{m}$ for which two different spray flame structures exist for the two smaller dropelt sizes and a single one for $R_0 = 50\,\mu\text{m}$. Figure 3 shows the spray flame structures for $R_0 = 10\,\mu\text{m}$, where the left part presents the flame with two chemical reaction zones and the right side that with a single reaction zone that resides on the spray side of the counterflow configuration. As the initial droplet radius is increased to $30\,\mu\text{m}$, see Fig. 4, the droplets penetrate deeper towards the gas side due to their increased momentum, which eventually leads to the chemical reaction zone to reside on the gas side of the configuration in the structure with a single chemical reaction zone, cf. Fig. 4b.

The flame structures for an initial droplet radius $30\,\mu\text{m}$ are also characterized by droplet reversal that does not exist for the flame structures of $10\,\mu\text{m}$ initial droplet radius. Droplet reversal and oscillation for larger droplets and higher gas strain rates are typical for spray flames in the counterflow configuation [14], and they dominate the spray flame structures. At an even higher intitial droplet radius of $50\,\mu\text{m}$, this leads to the non-existence of the flame structure with a single chemical reaction zone and only one unique numerical solution is obtained, see Fig. 5.

A comparison of the three structures with two chemical reaction zones for initial droplet radii of $10\,\mu\text{m}$, $30\,\mu\text{m}$, and $50\,\mu\text{m}$ reveals that the local minimum in the gas temperature profile considerably increases, which is a consequence of the droplet reversal and oscillation in this region, which enhances the combustion since the flame is fed with additional gaseous fuel due to vaporization.

In summary, it is concluded that the spray flame structures with two chemical reaction zones are the most stable as is visible from the regime diagrams displayed in Fig. 1. The single spray flame structures on the spray side of the configuration show the same characteristics as the

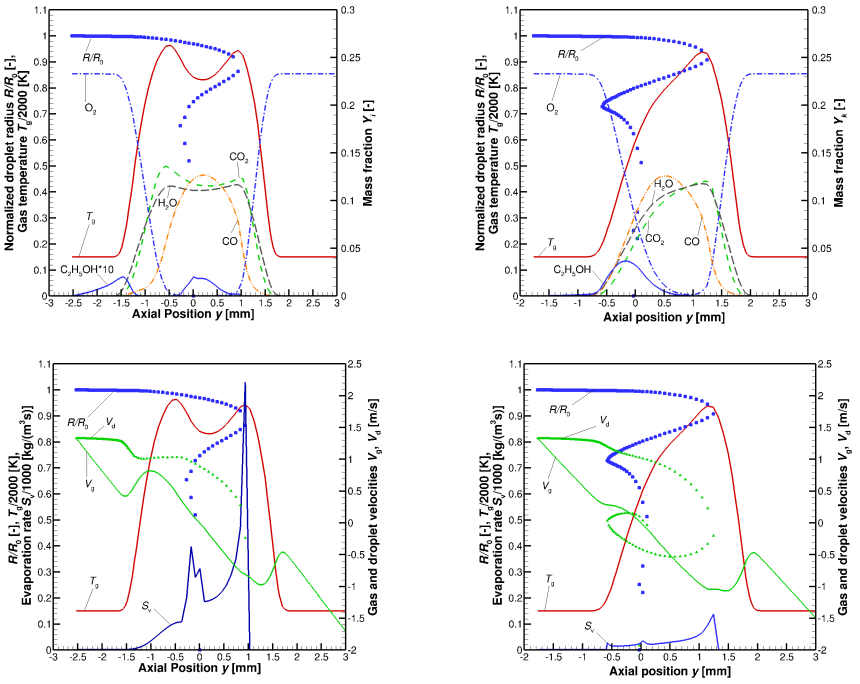

(a) Two reaction zones

(b) Single reaction zone on the gas side

Figure 4. Multiple spray flame structures for $R_0 = 30\,\mu\text{m}$, $E_\text{r} = 1.4$, $T_{\text{l},0} = T_{\text{g},0}$ = 300 K, $a_{-\infty}$ = 500/s. Upper part: Outer flame structure; Lower part: Spray characteristics.

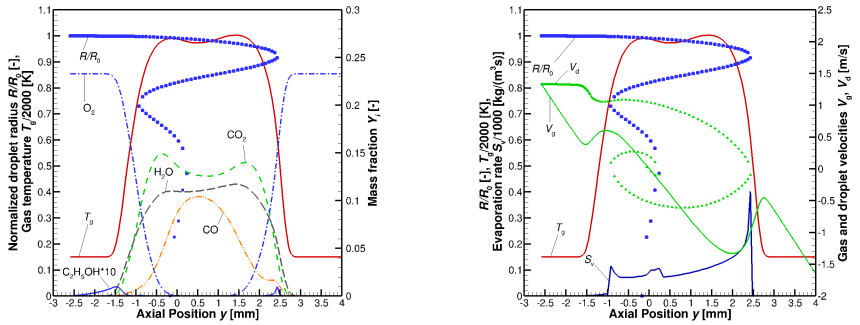

(a) Outer flame structure

(b) Spray characteristics

Figure 5. Multiple spray flame structures with two reaction zones for $R_0 = 50\,\mu\text{m}$, $E_\text{r} = 1.4$, $T_{\text{l},0} = T_{\text{g},0}$ = 300 K, $a_{-\infty}$ = 500/s.

spray-sided reaction zone in the two-reaction zone structures, which confirms the finding of Gutheil [9] for stoichiometric spray flames. The spray flame structure with a single chemical reaction zone on the gas side of the counterflow configuration shows a large separation of the vaporization and the chemical reaction zones [13] and does not show similarity to the gas-sided chemical reaction zone in the spray flames with two chemical reaction zones – this makes the flame structure most interesting also in the context of flame pulsation and micro-explosion of droplets as discussed by Ying et al. [13]. There are regimes in which even all three discussed spray flame structures coexist, see Fig. 1, but these triple flame structures exist only for small initial droplet radii and moderate gas strain rates.

Conclusions

Multiple structures of laminar fuel-rich ethanol/air spray flames in the counterflow configuration are studied numerically. Up to three different flame structures are found for the same initial and boundary conditions. Two different spray flame structures with a single chemical reaction zone either on the spray or the gas side of the counterflow configuration are identified, and a third spray flame structure consists of two chemical reaction zones on either side of the stagnation

plane. The spray flame structures with two chemical reaction zones are most stable. For small initial droplet size, the flame with the spray-sided reaction zone is more stable than that on the gas side whereas for larger initial droplet size, this is reversed due to the higher momentum of the larger droplets that penetrate deeper into the counterflow configuration. The conditions under which the mentioned multiple flame structures coexist are analyzed and discussed.

Acknowledgements
We gratefully acknowledge the financial support of the German Research Foundation (DFG) through SPP 1980, grant GU 255/13-2.

References

[1] P. Durand, M. Gorokhovski, and R. Borghi. An application of the probability density function model to diesel engine combustion. *Combustion Science and Technology*, 144(1-6):47–78, 1999.

[2] C. Hollmann and E. Gutheil. Flamelet-modeling of turbulent spray diffusion flames based on a laminar spray flame library. *Combustion Science and Technology*, 135(1-6):175–192, 1998.

[3] Y. Hu, H. Olguin, and E. Gutheil. A spray flamelet/progress variable approach combined with a transported joint pdf model for turbulent spray flames. *Combustion Theory and Modelling*, 21(3):1–28, 2017.

[4] N. Peters. *Turbulent Combustion*. Cambridge University Press, 2000.

[5] D. Carbonell, C.D. Perez-Segarra, P.J. Coelho, and A. Oliva. Flamelet mathematical models for non-premixed laminar combustion. *Combustion and Flame*, 156(2):334–347, 2009.

[6] H. Xu, F. Hunger, M. Vascellari, and C. Hasse. A consistent flamelet formulation for a reacting char particle considering curvature effects. *Combustion and Flame*, 160(11): 2540–2558, 2013.

[7] H. Barths, C. Hasse, and N. Peters. Computational fluid dynamics modelling of non-premixed combustion in direct injection diesel engines. *International Journal of Engine Research*, 1(3):249–267, 2000.

[8] G. Continillo and W.A. Sirignano. Counterflow spray combustion modeling. *Combustion and Flame*, 81(3):325–340, 1990.

[9] E. Gutheil. Multiple solutions for structures of laminar counterflow spray flames. *Progress in Computational Fluid Dynamics*, 5(7):414–419, 2005.

[10] A. Vié, B. Franzelli, Y. Gao, T. Lu, H. Wang, and M. Ihme. Analysis of segregation and bifurcation in turbulent spray flames: A 3d counterflow configuration. *Proceedings of the Combustion Institute*, 35(2):1675–1683, 2015.

[11] W. Xie, P.B. Govindaraju, Z. Ren, and M. Ihme. Structural analysis and regime diagrams of laminar counterflow spray flames with low-temperature chemistry. *Proceedings of the Combustion Institute*, 38(2):3193–3200, 2021.

[12] J. Carpio, D. Martínez-Ruiz, A. Liñán, A.L. Sánchez, and F.A. Williams. Hysteresis in the vaporization-controlled inertial regime of nonpremixed counterflow spray combustion. *Combustion Science and Technology*, 192(3):433–456, 2019.

[13] Z. Ying, H. Olguin, and E. Gutheil. Multiple structures of laminar fuel-rich spray flames in the counterflow configuration. *Combustion and Flame*, page 111997, 2022. in press.

[14] E. Gutheil and W.A. Sirignano. Counterflow spray combustion modeling with detailed transport and detailed chemistry. *Combustion and Flame*, 113(1):92–105, 1998.